Using Experimental Information to Produce a Model of the Transmembrane Domain of the Ion Channel Phospholamban

Pawel Herzyk and Roderick E. Hubbard
Department of Chemistry, University of York, Heslington, York YO1 5DD, England

ABSTRACT Molecular models of the transmembrane domain of the phospholamban pentamer have been generated by a computational method that uses the experimentally measured effects of systematic single-site mutations as a guiding force in the modeling procedure. This method makes the assumptions that 1) the phospholamban transmembrane domain is a parallel five-helix bundle, and 2) nondisruptive mutation positions are lipid exposed, whereas 3) disruptive or partially disruptive mutations are not. Our procedure requires substantially less computer time than systematic search methods, allowing rapid assessment of the effects of different experimental results on the helix arrangement. The effectiveness of the approach is investigated in test calculations on two helix-dimer systems of known structure. Two independently derived sets of mutagenesis data were used to define the restraints for generating models of phospholamban. Both resulting models are left-handed, highly symmetrical pentamers. Although the overall bundle geometry is very similar in the two models, the orientation of individual helices differs by ~50°, resulting in different sets of residues facing the pore. This demonstrates how differences in restraints can have an effect on the model structures generated, and how the violation of these restraints can identify inconsistent experimental data.

INTRODUCTION

Integral membrane proteins are a widely distributed and diverse group of proteins responsible for many important processes in intercellular communication and selective transport. Our understanding of the sequence, biology, and biochemistry of these proteins is increasing rapidly. However, the difficulties of producing active proteins in large quantities and their insolubility in polar solvents means that structural information is available only for a few special cases where the natural abundance and/or homogeneity of protein have facilitated the growth of suitable crystals. In the absence of direct experimental structural information, there continues to be considerable interest in the development and application of molecular modeling techniques for understanding the structure of these proteins and relating it to their function.

The lack of experimentally determined structures for most of the classes of membrane proteins means that there are not suitable templates that can be used with the established techniques of homology modeling to generate structural models. There is therefore a need for alternative modeling approaches in which the available experimental biological and biophysical data are used as a guiding force in the modeling process. We have previously described a computational methodology that generates models of seven-helix transmembrane (7TM) proteins on the basis of diverse experimental information (Herzyk and Hubbard, 1995). In this paper we demonstrate how these methods can be applied to the generation of models for parallel helix bundles on the basis of mutagenesis data and some simple assumptions about helix-bundle geometry.

Our model system, phospholamban (PLN), is a noncovalent homopentameric membrane protein localized in the membrane of the cardiac sarcoplasmic reticulum (SR) (Kirchberger et al., 1975). In its dephosphorylated state, PLN inhibits the steady-state activity of the Ca^{2+}-ATPase, whereas β-adrenergic stimulation results in cAMP- and calmodulin-dependent phosphorylation of PLN, which restores the full activity of the pump (Tada and Kadoma, 1989).

The PLN monomer consists of 52 amino acid residues, with an N-terminal stretch of 30 hydrophilic residues followed by a C-terminal stretch of 22 hydrophobic residues. The high helical content in PLN and, in particular, the 27-residue-long C-terminal tryptic fragment (QNLQNLFINFCLILICLLLICIIVMLL, residues 26–52) was demonstrated by circular dichroism (CD) in detergents (Simmerman et al., 1989) and CD and Fourier transform infrared (FTIR) studies of PLN in lipid bilayers (Arkin et al., 1995; Ludlam et al., 1996). In contrast to the 2–25 domain, both PLN and the 26–52 domain show Ca^{2+}-selective conductance in reconstituted lipid membranes (Kovacs et al., 1988), suggesting an alternative but not necessarily exclusive mechanism whereby PLN generates a passive calcium leak across the cardiac SR membrane. Although there is some debate regarding the function of PLN as an ion channel (Reddy et al., 1995), the calculations performed in this study assume that the transmembrane (TM) domain of PLN acts as an ion channel. Consequently, its pore-forming transmembrane domain is assumed to be a five-helix bundle, where each helix is a part of the C-terminal domain of residues 26–52.

A model of this pore-forming domain has been proposed by Brünger and co-workers (Adams et al., 1995) as a result

Received for publication 9 June 1997 and in final form 25 November 1997.
Address reprint requests to Dr. Pawel Herzyk, Department of Chemistry, University of York, Heslington, York YO1 5DD, England. Tel.: 44-1904-43-2593; Fax: 44-1904-410-519; E-mail: pavel@yorvic.york.ac.uk.

0006-3495/98/03/1203/12 $2.00

of a constrained global search conducted through a series of molecular dynamics simulated annealing (MDSA) calculations, including extensive searches for helix interactions. These assumed that the transmembrane domain is a five-helix bundle, each helix being a 35–52 stretch of 18 C-terminal hydrophobic residues. In that work it was explicitly stated that although it was possible to limit the number of models using an extensive search method, no simple criteria were capable of determining which model was most appropriate. As a result, the final model was selected on the criterion that it satisfied the available mutagenesis data (Arkin et al., 1994).

Our modeling technique (Herzyk and Hubbard, 1995) can be regarded as an inversion of the MDSA procedure. Instead of performing a thorough and time-consuming conformational search and then selecting the best solution on the basis of experimental data, we use the experimental data directly in the modeling process to generate model structures. The available experimental evidence is converted into structural restraints between different parts of the protein model. In the first stage of our procedure, the protein is represented as rigid helical units whose positions and orientations are optimized by a Monte Carlo simulated annealing procedure using the structural restraints in a target function. The resulting simplified template is then refined into a full-atom representation.

In this paper the effectiveness of these methods for parallel helix bundles is demonstrated through calculations for systems of known structure consisting of helix dimers. In the first set of calculations, the known structure of a leucine zipper from GCN4 is used to generate model mutagenesis data, which are then used to characterize the performance of the computational procedure in regenerating the helix dimer. This is followed by calculations in which real experimental mutagenesis data are used to generate models for the transmembrane domain of the dimeric protein glycophorin A. The modeling procedures are then applied to generate models of phospholamban on the basis of two independently generated sets of mutation data (Arkin et al., 1994; Simmerman et al., 1996).

METHODS

Generation of a simplified template model

The methods used for generating simplified models of the structure of membrane proteins has been described extensively elsewhere (Herzyk and Hubbard, 1995). In summary, the procedure consists of the following steps.

Defining a simplified representation of the protein as an aggregation of a number of rigid idealized helices

Each residue in the helix is represented by one C_α atom and one virtual side-chain atom, the size and position of which depend on the size and topology of the side chain. This is a simplified version of our earlier reduced representation for proteins (Herzyk and Hubbard, 1993). Two dummy atoms labeled DS and DI represent, respectively, the sarcoplasmic and intracellular ends of the helix. These dummy atoms can be used as anchor points for certain restraints, but do not take part in the steric overlap calculation.

Defining a set of structural restraints

Although five types of restraints were employed for modeling GPCRs (Herzyk and Hubbard, 1995), here we use only two of them:

1. *Distance restraints* are imposed between the ends of different helices in the bundle to prevent them from drifting away or collapsing into the pore. The restraints are imposed on DI-DI and DS-DS distances between dummy atoms of neighboring (1–2) helices and (1–3) helices (Kerr et al., 1994) (see Fig. 1). For (1–2) helices the lower and upper limits of restraints are set to 7 Å and 11 Å, whereas for (1–3) helices these limits are set to 11.3 Å and 17.8 Å, respectively. These values were inferred from analysis of the results of parallel helix bundles modeled by Sansom and co-workers (Kerr et al., 1994).

2. *Orientation restraints* are used to restrain certain residues to be either pointing inside (ORI-inside restraints) or outside (ORI-outside restraints) a helix bundle. Here, contrary to the original paper (Herzyk and Hubbard, 1995), *inside* is defined as facing the pore space or the interhelical space. This is achieved by incrementing the β angle by 12.8° on each side (see Appendix B in Herzyk and Hubbard, 1995, for details). In this context, *outside* means not *inside*.

Construction of a penalty function to measure how well a model satisfies the structural restraints

A restraint is declared satisfied as long as it falls between lower and upper limits. If it does not, then a violation is calculated as

$$viol = |X - X_{\text{lim}}|$$

where X represents a restrained quantity and X_{lim} is one of the limits, whichever is nearer. Each violation is penalized by a square-well function, and all contributions are summed over the number of violated restraints,

$$restr = \Sigma\, K\, viol^2$$

where K represents a scaling constant. Wherever it is not specified otherwise, K is set to 50 $Å^{-2}$ for distance restraints and to 5 $Å^{-2}$ for orientation

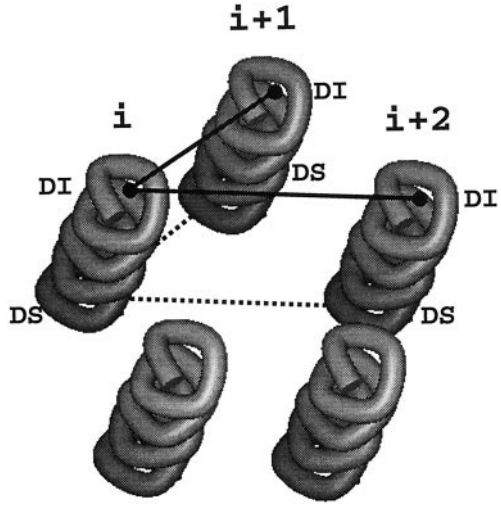

FIGURE 1 Schematic representation of distance restraints between (1–2) and (1–3) helices. For clarity, only restraints for one helix are presented.

restraints. The total penalty function P is given by

$$P = repel + restr$$

where *repel* describes the penalty for steric overlap.

Global optimization of the penalty function using the technique of Monte Carlo simulated annealing

Conformational searching starts at a high temperature and then continues as the system is cooled ("annealed") gradually and slowly. The term *temperature* refers to a parameter that regulates the acceptance rate in the Monte Carlo simulation (Kirkpatrick et al., 1983). A Monte Carlo simulated annealing (MCSA) trajectory is generated by initially producing a randomized configuration of rigid body elements representing the helices. For PLN, the five helices are arranged perpendicular to the membrane plane (xy plane) at the apices of a regular pentagon, 9.5 Å from its center, whereas for helix-dimer calculations they are positioned at the center of the coordinate system. The tilt of each helix with respect to the x and y axes are randomized within $\pm 45°$, and orientations relative to the z axis are randomized fully. This is followed by randomization of the x, y, and z coordinates of the centroid of each helix within a 2 Å boundary. After the initial configuration has been generated, each of the helices is moved sequentially by a random step of a randomly chosen coordinate (three translations and three rotations per rigid body element). After each random step, the increment in the penalty function is calculated, and the step is accepted or not on the basis of a Metropolis decision (Metropolis et al., 1953). One thousand such Monte Carlo steps are performed at each temperature as the temperature is lowered from the initial value of 8.0 by 10% in 25 steps. The first three temperature runs are carried out with the repulsive potential *repel* switched off.

Generation of final template

Fifty MCSA trajectories are generated for an ensemble of different initial configurations of the system. Final configurations with abnormally high penalty function values are discarded, and the mean structure is calculated by averaging the accepted final configurations. The final template is generated by superposition of idealized helices on the mean structure.

Refinement of the simplified template: conversion to a full atomic representation and geometry optimization

The simplified template created within the first stage is subjected to a molecular dynamics simulated annealing (MDSA) protocol to 1) extend it into a full-atom representation and to 2) optimize the geometry of the system. All calculations were carried out using the program X-PLOR (Brünger, 1992); the approach is similar to the protocol of Nilges and Brünger (1991). The protein is defined with a united atom and explicit polar hydrogen topology and parameter sets TOPH19 and PARAM19 (Brooks et al., 1983; Neria et al., 1996). Some modifications have been made so that all bonds, angles, and impropers have uniform energy constants of 500 kcal/mol Å^2, 500 kcal/mol rad^2, and 200 kcal/mol rad^2, respectively, and all planarities and chiralities are defined in terms of impropers rather than dihedrals. This is similar to how these terms are defined for NMR structural determination (Brünger, 1992). Because cysteine is the most polar residue in the stretch of 18 C-terminal residues, we have decided to keep the explicit γ-hydrogen. The appropriate parameters were adopted from a PARAM22 set (MacKerell et al., manuscript submitted for publication). The charges on helix N- and C-termini were neutralized.

The X-PLOR (Brünger, 1992) potential energy function contains restraint terms for bonds, angles, impropers, repulsive nonbonded or Lennard-Jones, electrostatics, and distances. Different combinations of these terms are used during different stages of the calculations. Two groups of distance restraints are used in the calculations. *Intrahelical distance restraints* are imposed on intrahelical hydrogen bond lengths. The distance between O(k) and N(k + 4) is kept between 2.4 Å and 3.2 Å, and the distance between O(k) and HN(k + 4) is kept between 1.7 Å and 2.3 Å. *Interhelical distance restraints* are imposed between adjacent helices by defining restraints between the pair of virtual atoms representing the termini of the helices, as illustrated in Fig. 1 for the simplified template. The centroid positions are the mean coordinates of the middle seven C_αs in each helix, and the termini positions are the mean coordinates of the first seven or last seven C_αs in each helix (Nilges and Brünger, 1991). The target distance ranges are kept the same as in the first stage of calculation.

The initial structure consists of the C_α positions from the simplified template with the other main-chain and side-chain atoms for each residue scattered randomly around the appropriate C_αs within a sphere of 1 Å diameter. This structure is then heated to 1000K, and several stages of molecular dynamics with a time step of 1 fs are performed at this temperature, keeping C_α atom positions fixed, as described by Nilges and Brünger (1991). During these stages different potential energy terms are introduced one by one (first bond and angle, then impropers, then repulsive nonbonded potential), and energy constants are significantly scaled down and then increased gradually to their maximum values (Nilges and Brünger, 1991). During this process the intrahelical restraints are used. The high temperature stage lasts for 10.3 ps. The system is then annealed to 300K for 2.9 ps by reducing the temperature of the heat bath by 25K every 0.1 ps. During this stage C_α atoms are released to be harmonically restrained to their initial positions with energy constants being reduced gradually. The repulsive nonbonded potential is replaced by Lennard-Jones and electrostatic potentials. A switching function is applied to both potentials between 8 Å and 12 Å, and a nonbonded neighbor list is generated within a radius of 13 Å; a distance-dependent dielectric constant ($\epsilon_{ij} = r_{ij}$ in Å) is used. During this stage both intrahelical and interhelical restraints are used. The annealing phase is then followed by a final burst of 5-ps dynamics at 300K, using the same set of restraints. The entire protocol is repeated 10 times (with different randomizations of initial side-chain atom position), and the mean structure is calculated. This structure is then finally minimized using no restraints.

Convergence

The convergence (*conv*) of the family of final structures generated within MCSA or MDSA protocols is measured by the average root mean square deviation (RMSD) from the mean structure over the family of selected structures overlapped on the main-chain atoms. Thus the lower the *conv* value, the higher (the better) the convergence.

Geometrical characterization of the final helix bundle

The helix-helix separations between adjacent helices in the bundle D are determined as the minimum distances between helix axes. Helix crossing angles Ω are determined according to the method of Chothia et al. (1981). In the case of PLN, both D and Ω are quoted as averaged over the five pairs of neighboring helices. R_{SYM} assesses the symmetry of a bundle as in Kerr et al. (1994):

$$R_{SYM} = \frac{1}{5}\sum_{i=1}^{4} RMSD_i$$

where $RMSD_i$ is the α-carbon RMSD between a bundle structure and the same structure in which helix 1 is relabeled as 1 + i, helix 2 as 2 + i, etc. Thus the lower the value of R_{SYM}, the higher the symmetry of the bundle.

Software

The simplified templates are calculated using the program PANDA (Herzyk and Hubbard, 1995). The refinement into the full-atom representation

uses the program X-PLOR, version 3.843 (Brünger, 1992). Display and examination of templates and refined models were performed with the programs SQUID (Oldfield, 1992), Molviewer (M. J. Hartshorn, unpublished program), and QUANTA (MSI, San Diego, CA).

RESULTS

In our earlier work on seven-helical proteins (Herzyk and Hubbard, 1995), a diverse set of experimental information was available to define a variety of restraints from which the MCSA protocol generated a structure. For the TM domain of phospholamban, only mutational data are available. The results of mutagenesis can be translated into structural restraints on the basis of the assumption that the sensitivity of a residue to an oligomer disruptive mutation is a measure of its involvement in interhelical interactions. Consequently, sensitive residues are assumed to be facing inside the bundle and vice versa. These orientational restraints are combined with distance restraints between helix ends generated to prevent the helices from drifting away or collapsing into the pore. In an initial set of calculations, we assessed how well this computational procedure worked in reproducing the structure of two helix dimers whose structure had been determined experimentally. The first example is the GCN4 leucine zipper, where the known structure is analyzed to generate a model set of mutagenesis data, which are then applied in calculations to produce a model structure. The second example is for the glycophorin A transmembrane domain, where real experimental data on the effects of mutagenesis are available.

GCN4 leucine zipper

The structure of a peptide corresponding to the leucine zipper of the transcriptional activator GCN4 has been determined by x-ray crystallography at 1.8-Å resolution (O'Shea et al., 1991; PDB code 2zta, Bernstein et al., 1977). It shows a two-stranded, left-handed coiled coil of parallel, identical, 31-residue-long α-helices with the sequence Ac-RMKQLEDKVEELLSKNYHLENEVARLKKLVG-COO. From this structure we have derived simulated mutational data based on the estimations of the average, interhelical van der Waals energy per residue. Consequently, residues with interaction energies close to zero were oriented *outside* (residues K3, Q4, D7, E10, E11, S14, Y17, H18, N21, A24, R25, K28, and G31), whereas all others were oriented *inside*. This gives, for the dimer, a total of 26 ORI-outside and 36 ORI-inside restraints. In addition, two distance restraints are imposed between the corresponding ends of the helices represented by DI and DS atoms, to keep them between 7 Å and 11 Å apart (see Methods).

Fifty MCSA trajectories were generated, all of which converged to a single structure with a *conv* value of 0.1 Å (Fig. 2 *A*). The RMSD for C_α atoms between the final template and the 2zta structure, disregarding the first and the last residues, is only 1.07 Å. The refinement of the final template produced a family of 10 all-atom structures characterized by a *conv* value of 0.94 Å calculated on main-chain atoms (Fig. 2 *B*). The final GCN4 leucine zipper model is very close to the 2zta structure (Fig. 2 *C*). The RMSD for the 2–30 stretch is 0.97 Å on the main-chain atoms, and 1.16 Å on the main chain and all atoms of residues buried in the dimerization interface, namely, M2, L5, V9, L12, N16, L19, V23, L26, and V30. Interestingly, a virtually identical template (RMSD = 0.24 Å) was calculated if only ORI-inside restraints concerning the above nine residues were used.

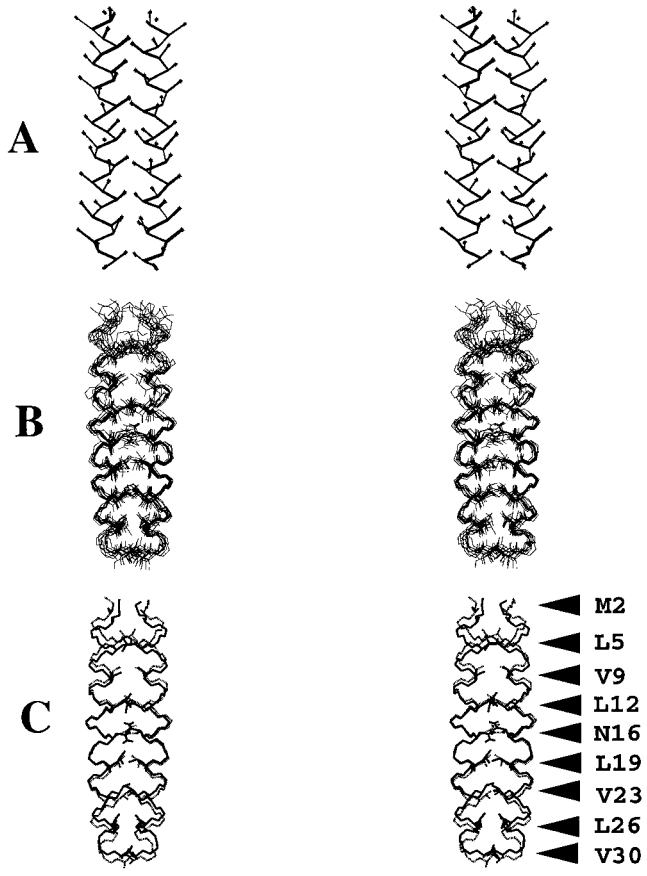

FIGURE 2 Graphical representation of model generation for the GCN4 leucine zipper. (*A*) Wall-eyed stereo plot of the accepted 50 final configurations (overlapped on C_α atoms) generated by MCSA calculations and used in calculating the final simplified template. (*B*) Wall-eyed stereo plot of the final family of 10 accepted refined structures, overlapped on the main-chain atoms, and used in the final structure calculation; only backbone and residues making up the dimerization interface are shown. (*C*) Wall-eyed stereo plot of the final model (*solid line*) and crystal structure (PDB code 2zta) (O'Shea et al., 1991) (*dashed line*) overlapped on the main-chain atoms. Only backbone and residues making up the dimerization interface (*highlighted*) are shown.

Dimer of glycophorin A TM domain

It has been shown by in vitro experiments that glycophorin A (GpA) from human erythrocytes dimerizes through specific interactions mediated by its single TM α-helices (Bormann et al., 1989). Recently the structure of the TM domain

of the GpA dimer in sodium dodecyl sulfate micelles has been determined by NMR (MacKenzie et al., 1997; PDB code 1afo, Bernstein et al., 1977). It showed that the α-helices formed by residues 73–96 create a right-handed dimer with the relatively high crossing angle of $\Omega = -40°$.

In a comprehensive site-directed mutagenesis study, each of the amino acids in the helix was substituted with the nonpolar residues A, C, V, L, I, M, F, and W (Lemmon et al., 1992), and the effects on helix-helix association were measured. In this study we concentrate on the 18-residue peptide 74–91 (TLIIFGVMAGVIGTILLI), which is well inside the TM region, and for which the effects of substitution were the strongest. The same region was also used in earlier modeling studies of Brünger and co-workers (Adams et al., 1996; Treutlein et al., 1992), where a global search of the interhelical interactions was performed, and the final models were assessed on the basis of the mutation data (Lemmon et al., 1992). The coordinate set for the final model in that study (Adams et al., 1996) was deposited in the Brookhaven data base (Bernstein et al., 1977) with the code 1msr.

In the models generated here, orientation restraints were derived from the mutational data. For each residue that was mutated, we have calculated the relative number of disruptive mutants P_i as defined by Treutlein et al. (1992). Residues with P_i equal to zero were assumed to be oriented *outside* (T74, F78, M81, A82, and I85), whereas residues with P_i greater than 2 were assumed to be oriented *inside* (L75, I76, G79, V80, G83, V84, and T87). The remaining residues whose P_i value was higher than zero but lower than 1.3 were not restrained. Thus in total we have 10 ORI-outside and 14 ORI-inside restraints, as well as two distance restraints imposed on the distances between corresponding helix ends represented by DI and DS atoms, to keep them between 7 Å and 11 Å apart (see Methods).

Fifty MCSA trajectories were calculated, all of which converged to a single configuration with a *conv* of 0.07 Å (Fig. 3 *A*). The final template is a right-handed dimer, very similar to both 1afo (MacKenzie et al., 1997) and 1msr models (Adams et al., 1996), with an RMSD of 0.93 Å and 0.68 Å, respectively. An identical template (RMSD = 0.01 Å) was generated if only ORI-inside restraints were used. The final model was generated from the family of 10 structures (Fig. 3 *B*) calculated with the MDSA protocol. Its comparison with the 1afo model is presented in Fig. 3 *C*. The RMSD between the 75–90 stretches of these two structures is 0.91 Å and 1.35 Å on main chain and all-atoms, respectively.

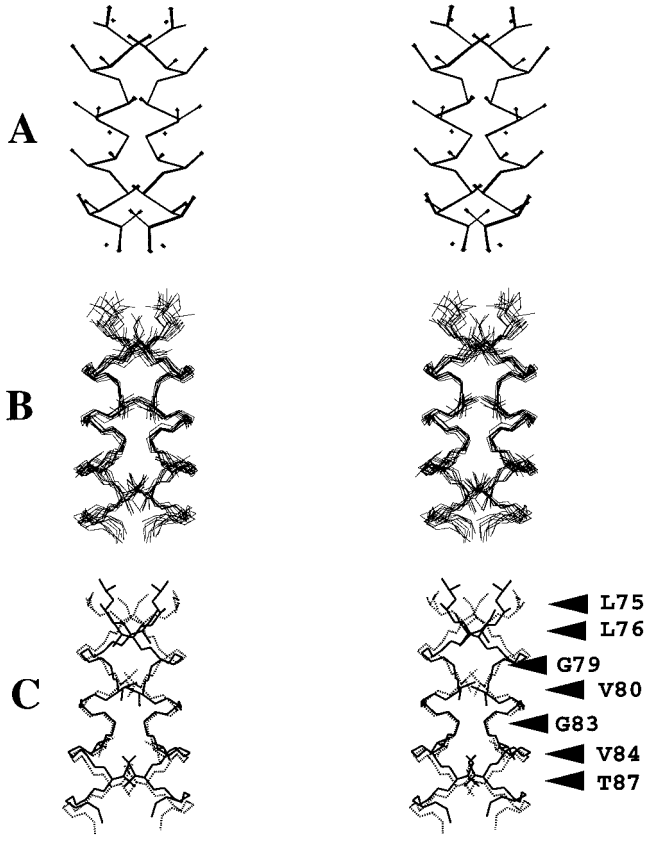

FIGURE 3 Graphical representation of model generation for the transmembrane domain of glycophorin A. (*A*) Wall-eyed stereo plot of accepted 50 final configurations (overlapped on C_α atoms) generated by MCSA calculations and used in calculating the final simplified template. (*B*) Wall-eyed stereo plot of the final family of 10 accepted refined structures, overlapped on the main-chain atoms, and used in the final structure calculation; only backbone and residues making up the dimerization interface are presented. (*C*) Wall-eyed stereo plot of the final model (*solid line*) and the mean NMR structure (PDB code 1afo) (MacKenzie et al., 1997) (*dashed line*) overlapped on the main-chain atoms. Only backbone and the residues making up the dimerization interface (highlighted) are presented.

Model of the transmembrane domain of PLN pentamer

Source of experimentally driven structural restraints

Two groups have reported independent studies that measure the effect of site-directed mutagenesis at positions along the TM domain of the PLN pentamer (Arkin et al., 1994; Simmerman et al., 1996). The results of these experiments are here used to generate two sets of orientation restraints.

In the first study (Arkin et al., 1994), each residue of the 35–52 C-terminal stretch (FCLILICLLLICIIVMLL) of the human PLN sequence was separately mutated into a number of residues (G, A, S, C, T, V, I, L, M, F), and the ability of each mutant to form pentameric complexes in sodium dodecyl sulfate-polyacrylamide gel electrophoresis was determined. The residue positions were classified as disruptive (37, 40, 44, and 47), partially disruptive (36, 39, 41, 43, 46, 49, and 51), and nondisruptive (35, 38, 42, 45, 48, 50, and 52). In our modeling, residues occupying nondisruptive positions are oriented *outside*, whereas residues occupying disruptive and partially disruptive positions are oriented *inside* (see Methods). Thus in total we have 55 ORI-inside and 35 ORI-outside restraints in this data set, termed ARK-1 (Table 1).

In the second study (Simmerman et al., 1996), each of the C-terminal amino acids at positions 26 to 52 were separately

TABLE 1 Characterization of different data systems for several MCSA calculations of phospholamban

Data system	Residue positions oriented inside the helix bundle	Residue positions oriented outside the helix bundle	Final template*
ARK-1	36 37 39 40 41 43 44 46 47 49 51	35 38 42 45 48 50 52	A
ARK-2	36 37 39 40 41 43 44 46 47 50 51	35 38 42 45 48 49 52	A
ARK-3	36 37 40 41 43 44 47 50 51	35 38 39 42 45 46 48 49 52	S
SIM-1	37 40 41 44 47 50 51	35 38 42 45 48 49 52	S

*Geometry of the final template. A, Similar to the ARK-1 template; S, similar to the SIM-1 template.

replaced by Ala and Phe, and the ability of the mutant to pentamerize was assessed in the same way as in Arkin et al. (1994). If we confine ourselves to the 35–52 stretch, then the assumption is made that a particular residue position is declared disruptive if at least one of two mutations is disruptive, which is the case for residue positions 37, 40, 41, 44, 47, 50, and 51 (see table 1 in Simmerman et al., 1996). A residue position is declared nondisruptive if both mutations are nondisruptive, which occurred for residue positions 35, 38, 42, 45, 48, 49, and 52. The effect of mutations at the remaining four residues (36, 39, 43, and 46) was inconclusive, and no restraints were assigned. Thus this data set, termed SIM-1, contains 35 ORI-inside and 35 ORI-outside restraints (Table 1).

For both set of restraints, an additional 20 distance restraints are imposed between dummy atoms representing the helix ends of neighboring (1–2) and (1–3) helices (see Methods). A model system of five α-helical, 18-residue-long helices representing residues 35–52 was used.

PLN TM domain model on the basis of the Arkin mutagenesis data

Forty-eight of fifty final MCSA configurations generated for the ARK-1 system (Table 1) converged on a single structure with a value for *conv* of 0.18 Å and with penalty function values between 330 and 336. The final simplified ARK-1 template is a left-handed pentamer whose geometrical parameters are presented in Table 2. A refined full-atom ARK-1 model was then generated using the MDSA protocol. Ten structures were calculated, and all of them were accepted. The structures show high convergence (Table 2) and produced a model consisting of a parallel helix bundle corresponding to a left-handed coiled-coil.

A comparison of the ARK-1 model and the Adams model (Brookhaven code, 1psl; Adams et al., 1995) is made in Fig. 4 *A*, showing that the models have very similar geometries. The interhelical separation D is 9.8 Å and 9.4 Å, and the helical crossing angle Ω is 15.3° and 18.2° for the ARK-1 and 1psl, respectively. It can be seen from Fig. 4 that helix orientations (with respect to their long axes) are virtually identical, and the main difference between the two models is caused by some helix displacements in the direction perpendicular to the membrane. This can be measured by the symmetry of the bundle measured as R_{SYM} of 0.26 Å for the ARK-1 model, which is more symmetrical than the value of 1.02 Å for the 1psl model.

Additional calculations were made for a system containing a 23-residue TM domain equivalent to residues 30–52 (NLFINFCLILICLLLICIIVMLL), using the same ARK-1 data set. The common parts of the full-atom models are essentially identical, with RMSD of 0.30 Å and 0.65 Å on the main chain and all-atoms (Fig. 4 *B*). This is important, as it shows that a decision on where to assign the beginning of the helix does not affect the performance of the techniques.

PLN TM domain model on the basis of the Simmerman mutagenesis data

Forty-nine of fifty final MCSA configurations calculated for the SIM-1 data set (Table 1) converged well (Fig. 5 *A*) with *conv* of 0.44 Å and penalty function values between 20.1 and 24.1. The final SIM-1 template is a left-handed pentamer. The full-atom SIM-1 model was generated after 10 final structures calculated with the MDSA protocol were averaged (Fig. 5 *B*). The SIM-1 model is a bundle corresponding to a left-handed coiled-coil, and its geometrical parameters are presented in Table 2.

TABLE 2 Geometric characterization of final simplified templates and final refined models

	ARK-1		SIM-1	
Parameter*	Template	Model	Template	Model
conv (Å)	0.18	0.56	0.44	0.70
$RMSD_{ref}$ (Å)#	0.96	0.94/1.33	2.02	1.51/2.78
R_{SYM} (Å)	0.04	0.26	0.04	0.26
D (Å)	9.2	9.8	9.7	9.6
Ω (°)	22.1	15.3	18.1	16.1

*For a description of these parameters, see Methods.

#RMSD from the reference structure. For the ARK-1 template and model, the reference structure is the 1psl model (Adams et al., 1995); for the SIM-1 template and model, these are the ARK-1 template and model, respectively. The RMSD values for simplified templates are calculated over C_α atoms, whereas for refined models over main-chain and all-atoms, respectively, they are calculated excluding the first and last residues.

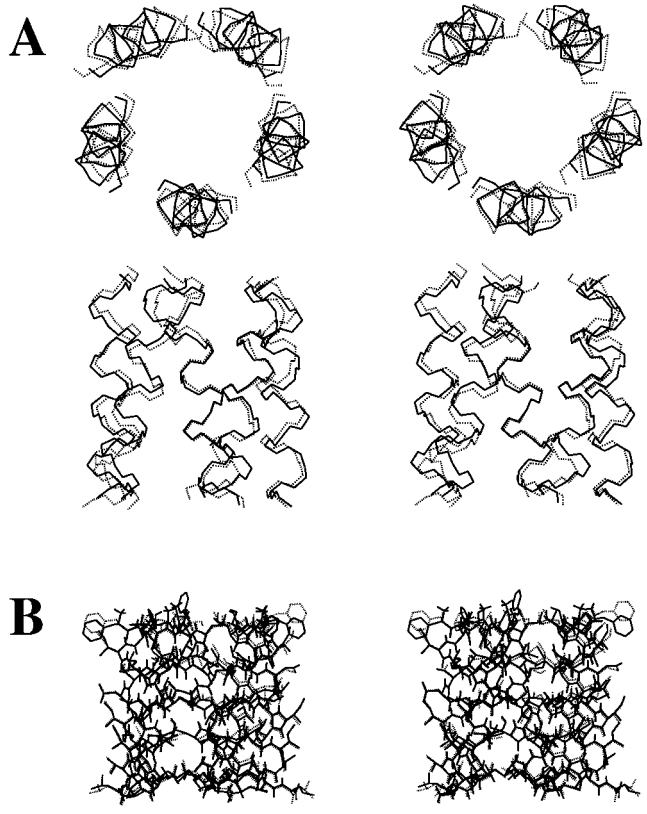

FIGURE 4 Graphical representation of the similarities between different models of the transmembrane domain of PLN using the ARK-1 data system. (*A*) Orthogonal wall-eyed stereo view of the main chains of the 36–51 domain of the final ARK-1 model (*solid line*) and 1psl model (Adams et al., 1995) (*dashed line*) overlapped on the main-chain atoms. The upper panel shows a view from the cytosolic side; the lower panel shows a side view with the cytosolic side at the top. (*B*) Wall-eyed stereo plot of the common parts of the ARK-1 model (*solid line*) and the model generated using the same ARK-1 data set but longer helices (30–52 stretch) (*dashed line*) overlapped on main-chain atoms (cytosolic side at the *top*).

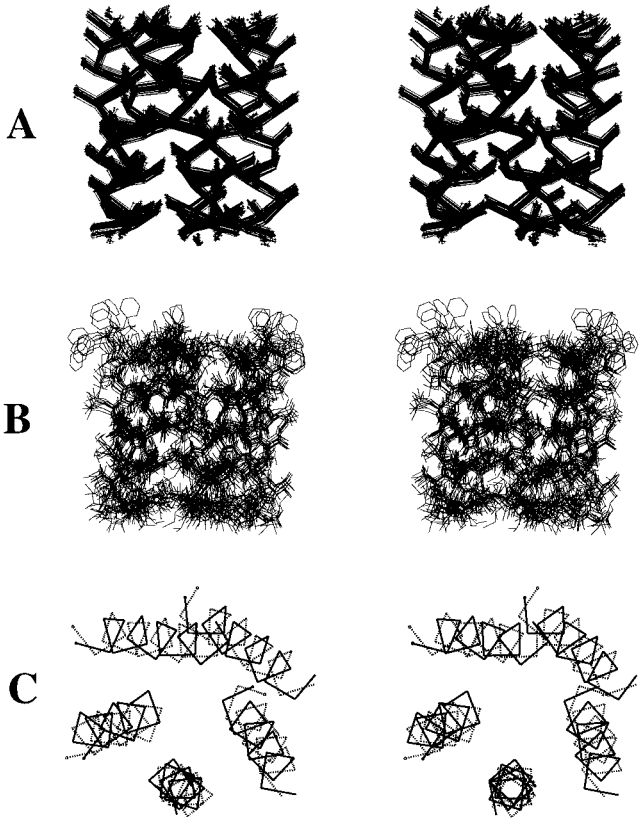

FIGURE 5 Graphical representation of the generation of the model for the transmembrane domain of PLN using the SIM-1 data set. (*A*) Wall-eyed stereo plot of accepted 49 final configurations (overlapped on C_α atoms) generated by the MCSA calculations and used in the final simplified template calculation (cytosolic side at the top). (*B*) Wall-eyed stereo plot of the final family of 10 accepted refined structures, overlapped on the main-chain atoms, and used in the final structure calculation (cytosolic side at the *top*). (*C*) Wall-eyed stereo plot of the main chains of the 36–51 domain of the final SIM-1 model (*solid line*) and the ARK-1 model (*dashed line*) overlapped on the main-chain atoms (view from the cytosolic side).

Comparison of the ARK-1 and the SIM-1 models

Fig. 6 shows a plot of the averaged, interhelical van der Waals energy per residue for the final models of both the ARK-1 and SIM-1 systems. Both show a characteristic heptadic interhelical interaction pattern, which is shifted by four residues from one model to the other. This pattern is best visible for the 38–45 domain in the case of the ARK-1 system and the 42–49 domain in the case of the SIM-1 system. Small perturbations occur at positions 36 and 46 in the ARK-1 pattern and at 36 and 41 in the SIM-1 patterns (Fig. 6), respectively. These residues are cysteines, which seem to be too small to match the "knob-into-hole" pattern. A direct comparison of the final models as well as the final templates demonstrates that in the SIM-1 model, each helix is rotated counterclockwise by ~360°/7 as viewed from the cytosolic side (Fig. 5 *C*). Consequently, the residues that make up the pore surface are not the same in both models, namely L37, I40, L44, I47, and L51 in the SIM-1 model and C36, I40, L43, I47, and M50 in the ARK-1 model. The overall geometries of the bundle in the two models are essentially identical (Table 2) and consistent with results on pentameric bundles of parallel, model hydrophobic helices (Kerr et al., 1994) and the recent crystal structure of the five-stranded coiled-coil in cartilage oligomeric matrix protein (COMP) (Malashkevich et al., 1996).

Why do similar experimental data produce different models?

Although the mutation data of Arkin (Arkin et al., 1994) and Simmerman (Simmerman et al., 1996), described briefly above, are similar, they are by no means identical. Several calculations were performed with slightly different interpretations of the mutagenesis data to identify the source of the inconsistencies in the models (Table 1).

A comparison of the SIM-1 and the ARK-1 data sets, presented in Table 1, shows that they are consistent for 12 of 18 residues. Residues F35, I38, L42, I45, I48, and L52

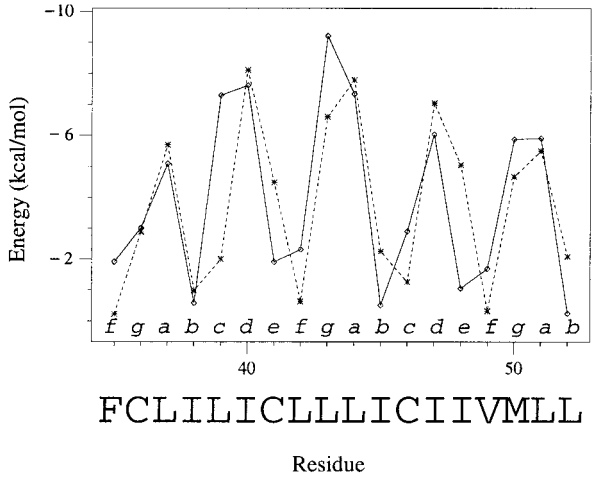

FIGURE 6 Interhelical van der Waals interaction energy per residue. ◇, ARK-1 model; *, SIM-1 model.

are all oriented *outside*, and residues L37, I40, C41, L44, I47, and L51 are oriented *inside*. The main difference is at residues V49 and M50. Position 50 is classified as nondisruptive in the ARK-1 set, as all four mutations M50G/A/S/T are nondisruptive. In the SIM-1 experiments, however, mutation M50F is clearly disruptive. This suggests that position 50 is at least partially disruptive and therefore should be oriented *inside* in both data sets. Mutations V49A/F are partially disruptive in the ARK-1 set and nondisruptive in the SIM-1 set. However, close inspection of the MCSA trajectories for the ARK-1 calculation reveals that the ORI-inside restraint imposed on V49 is the most violated, as this residue is clearly oriented *outside* in the final template. In addition, the final template for SIM-1 shows no violations for the V49 ORI-outside restraint. This analysis suggests that V49 should be oriented *outside* rather than *inside*.

MCSA calculations were then performed for the ARK-1 data set modified, so that V49 was oriented *outside* and M50 was oriented *inside* (the new restraint set and models are labeled ARK-2) (Table 1). Forty-nine final structures converged well with *conv* = 0.26 Å, and the final ARK-2 template is essentially identical to the ARK-1 final template, with an RMSD of only 0.19 Å. The penalty function values were greatly reduced and fell to between 128.2 and 132.6. So, although the changes in the restraints for V49 and M50 improved the agreement between the restraints and the model, it did not generate a model with the SIM-1 orientation.

These calculations suggest that the difference in the two models is caused by a difference in the interpretation of the mutation data for the remaining residues, C36, L39, L43, and C46. These residues are omitted from the ORI restraint list in the SIM-1 set, as the mutation data seem to be inconclusive and are oriented *inside* in the ARK-1 system, as they are classified as partially disruptive (Arkin et al., 1994). Close analysis of the ARK-1 and SIM-1 templates reveals that C36 and L43 face either the pore (ARK-1) or interhelical space (SIM-1); thus their locations are structurally similar in the two models with respect to the *inside-outside* division. Moreover, the Arkin data for L43 are strong, leaving no doubts that this residue should be oriented *inside*. However, the locations of residues L39 and C46 are different in the two models, as they both face interhelical space in the ARK-1 template and the lipid environment in the SIM-1 template. We therefore performed MCSA calculations, using the ARK-2 data set, modified so that the ORI-inside restraints for L39 and C46 are changed into ORI-outside restraints. This data set (called ARK-3) is equivalent to the SIM-1 data set, with inconclusive data interpreted so that C36 and L43 are oriented *inside* and L39 and C46 *outside* (Table 1). The final ARK-3 template is essentially identical to the SIM-1 final template, with an RMSD of 0.3 Å, to be compared with an RMSD from the ARK-1 template of 1.9 Å. Similar results are obtained if both ORI-inside restraints for L39 and C46 are simply omitted from the ARK-2 list. Thus reversing or omitting the two restraints for residues L39 and C46 in the Arkin mutation data switches the template generated to that generated by Simmerman's mutation data.

The ARK-2 and ARK-3 data sets have the same number of restraints, allowing the penalty functions to be compared. This shows that the penalty function for the ARK-2 template is 70% higher, due mainly to a high penalty for exposing C41 to the lipid environment. Both sets of mutation data show strong evidence for the importance of position 41 in the pentamerization process, which argues for restraining C41 *inside*. Thus the price for forcing L39 and C46 *inside* in the ARK-2 template is to expose C41 to the lipid environment.

DISCUSSION

The results presented in this work show that a computational method for generating models of membrane-bound proteins on the basis of limited experimental information, initially designed for modeling 7TM receptors (Herzyk and Hubbard, 1995), is also applicable to parallel helix bundles believed to be the pore-forming domains of ion channels.

The quality of the final structure depends on the quality of restraints. For these parallel helix bundles, two types of restraints have been used. The interhelical distance restraints arise from assumptions about the interhelical interaction and pore architecture. Rather than targeting an arbitrarily chosen distance value (Kerr et al., 1994), they are constructed to allow distances between neighboring and 1–3 helices to change freely within the range 4 Å and 6.5 Å, respectively. The main function of these restraints is to ensure that the helix bundle has been formed and that none of the helices collapse into the pore or drift away from the bundle. They do not exert artificial attractive forces between helices, which is the case when distance restraints aimed at a target value lower than the interhelical separation distance are applied (Kerr et al., 1994). The second group of restraints, orientation restraints, defines the lipid-exposed sur-

face of the helix bundle and drives the formation of a bundle with the correct tilts and orientations for the helices. The restraints assume that certain residues protrude outside the bundle and certain residues do not.

Although our methodology had been validated for 7TM proteins using bacteriorhodopsin as a test case (Herzyk and Hubbard, 1995), only limited restraint information is derived for the parallel helix bundle proteins. The series of calculations on helix dimer systems was therefore performed to assess how well these limited restraints can define a model structure.

The first test calculations used synthetic restraints derived from an analysis of the residues involved in helix packing in the known structure of the GCN4 leucine zipper. Residues that did not participate in interhelical interaction were assumed to be oriented *outside*, whereas all others were oriented *inside*. The success of this test (RMSD from crystal structure on main-chain atoms of less than 1 Å) also shows that using idealized, rigid helices at the first stage of the calculation is an acceptable simplification, even in the case where the real helices wrap around each other to form a left-handed supercoil.

The second set of calculations for the dimer of the TM domain of glycophorin A used real mutagenesis data (Lemmon et al., 1992). Here the assumption was made that mutations that do not disrupt dimerization involve residues that do not participate in the interhelical interaction and vice versa. The resulting models were again of very high quality, as demonstrated by atomic RMSD below 1 Å (on main-chain atoms) from the NMR model 1afo (MacKenzie et al., 1997). The computed model shows that the helices are separated by only 6.1 Å at the crossing point near G79, and the crossing angle is $-43°$. Our model is also consistent with the solid-state NMR measurements of two interhelical distances V80($^{13}CH_3$) ↔ G79($^{13}C{=}O$) and V84($^{13}CH_3$) ↔ G83($^{13}C{=}O$), which determines their upper limits as 6 Å (Smith and Bormann, 1995). In our model these distances are equal, on average, to 4.9 Å and 5.4 Å, respectively.

Brünger and co-workers used the molecular dynamics simulated annealing technique for a global search of the helix arrangements in the dimer of TM domains of GpA (Adams et al., 1996; Treutlein et al., 1992), and the final models were selected on the basis of comparison with the mutational data (Lemmon et al., 1992). These calculations, however, depended critically on the search protocol used, as the two studies produced two different models, of which only one, 1msr (Adams et al., 1996), is consistent with the NMR 2zta model (MacKenzie et al., 1997) and the solid-state measurements (Smith and Bormann, 1995). By contrast, our calculations generated the final correct solution directly.

These test calculations on helix-dimer systems demonstrate that it is reasonable to identify a residue as being involved in helix-helix interaction on the basis of the sensitivity of that position to dimer disruptive mutants. This information can be used to apply simple structural restraints where residues insensitive to mutations are oriented outside the interface area and those that are sensitive are oriented inside. These restraints, combined with the requirement for spatial proximity of two interacting helices, allow the construction of a simple function penalizing violations of the restraints. Global optimization of the penalty function, enhanced with a simple repulsive potential, allows the rapid generation of an optimal model structure that corresponds to the correct atomic model.

Two different sets of mutation experiments (Arkin et al., 1994; Simmerman et al., 1996) have been used to extract structural restraints for the TM domain of phospholamban and used to calculate models. The only assumptions made were that 1) the transmembrane domain is a parallel five-helix bundle, and 2) nondisruptive mutation positions are lipid exposed, whereas 3) disruptive or partially disruptive mutations are not. Previously, Adams and co-workers proposed a model of the PLN transmembrane domain from a constrained global search for optimal helix orientations and interhelical crossing angles (Adams et al., 1995). This search was performed by a series of MDSA calculations on both dimer and symmetric pentamer model systems in a full-atom representation, and the suggested correct model was selected on the basis of consistency with the Arkin mutagenesis data (Arkin et al., 1994). This contrasts markedly with our approach using MCSA procedures, where the search space is directly limited by the mutagenesis data. In addition, the MCSA calculations are very rapid (no more than a few seconds of computer time for one template), and multiple structure determinations converge on a single configuration when the structural restraints are consistent. The speed and reproducibility of the MCSA procedure allow the calculations to be performed many times, which is necessary for rapid evaluation of alternative interpretations of experimental data.

The models generated with the MCSA procedure for the Arkin mutagenesis (ARK-1) data are very similar to the Adams model (Adams et al., 1995). However, there are some important differences between these models and those generated using the Simmerman (SIM-1) mutation data. Models generated using the ARK-1 and SIM-1 data sets (Table 1) are five-stranded, left-handed parallel helix bundles of virtually identical geometry, as measured by the interhelical crossing angle and interhelical separation (Table 2). These parameters are consistent with those of the crystal structure of the pentameric COMP channel (Malashkevich et al., 1996). The main difference between the ARK-1 and SIM-1 models is that helices in the SIM-1 model are rotated around their long axes counterclockwise by $\sim 360°/7$, as viewed from the cytosolic side (Fig. 5 *C*).

A series of MCSA calculations using slightly altered original ARK-1 and SIM-1 data sets have identified the source of the inconsistencies in the models generated. Most differences can be attributed to the orientation restraints derived for the two residues L39 and C46, which gave inconclusive evidence in the Simmerman study, and were classified as partially disruptive in the Arkin study. A comparison of the penalty function values and restraint viola-

tions also shows that the templates built on the basis of the Arkin mutation data violate one of its important restraints and force C41 to be lipid exposed. Thus it seems that the Simmerman data are more consistent with their template, because of a lack of serious restraint violations, than the Arkin data are with their template.

Although the MCSA calculations of simplified templates can explain why different models have been created and which data set is more consistent with its template, they cannot determine which template is the correct one. For this purpose, the simplified templates are built into full-atom models, using a molecular dynamics procedure, and the interactions of the amino acid residues in these final models are subjected to more detailed analysis.

The left-handed coiled-coil geometry of the SIM-1 and ARK-1 models allows the α-helical residue positions to be classified into four groups, based on the positions *a–g* that the residues occupy on a helical wheel with a pitch of 3.5 residues per turn, as shown in Fig. 7 *A*. Group I is residues facing the pore. In the SIM-1 model they occupy positions *a* and *d* (Fig. 7 *B*), whereas in the ARK-1 model they are at positions *d* and *g* (Fig. 7 *C*). These residues are involved in interhelical interactions as shown in Fig. 6, and each of them interacts with residues from two neighboring helices. Group II is residues that face interhelical space but do not make up the pore surface. They occupy positions *e, g,* and *a, c* in the SIM-1 and ARK-1 models, respectively. These positions contribute significantly to interhelical interactions as shown in Fig. 6, and each of them interacts with residues from one neighboring helix. Only those residues from groups I and II make knobs in the interhelical "knobs-into-hole" interactions. Group III residues are lipid exposed and contribute to weak interhelical interactions. They occupy positions *b, c*, and *e, f* in the SIM-1 and ARK-1 models, respectively. Group IV residues are lipid exposed and do not participate in the helix-helix interactions. They occupy positions *f* and *b* in the SIM-1 and ARK-1 models, respectively, and are oriented in the direction opposite the center of the pore. This packing characteristic is fully consistent with the crystal structure of the COMP channel (Malashkevich et al., 1996).

The heptadic periodicity of both interhelical van der Waals energy profiles (Fig. 6) is characteristic of the left-handed coiled-coil packing and came out as a result of heptadic periodicity of some residues whose mutations were classified as nondisruptive or disruptive. This heptadic mutation pattern is stronger in the case of the SIM-1 data set (nondisruptive: 35/42/49, 38/45/52; disruptive: 37/44/51 and 40/47) as compared to the ARK-1 data set (nondisruptive: 35/42, 38/45/52; disruptive: residues 37/44 and 40/47). Using the SIM-1 heptadic mutation pattern, the authors of that study (Simmerman et al., 1996) proposed that the 37–52 stretch adopts a pentameric coiled-coil structure stabilized by a leucine-zipper motif formed by residues from fully disruptive positions, namely L37, I40, L44, I47, and L51. They suggested that the central pore be defined by the hydrophobic surfaces of those five residues. Although a structural model for the bundle was not presented, the proposed characteristics of the TM domain are consistent with the SIM-1 model, although the latter is stabilized equally by residues from groups I and II, at positions *a*, *d*, *e*, and *g*.

The most striking differences between the SIM-1 and ARK-1 final models is that in the SIM-1 model, the positions of the mutations classified consistently in both mutagenesis studies as disruptive face the pore, whereas in the ARK-1 model, I40 and I47 face the pore (group I, position *d*), and L37 and L44 face the interhelical space between neighboring helices (group II, position *a*). In fact, the fifth most important residue for pentamerization detected by Simmerman et al. (1996), L51, completes the set of residues belonging to group I in the SIM-1 model. Whichever model is correct, it should rationalize the selection of the position of the most disruptive mutations.

If the ARK-1 model was correct, then there should be an explanation for the division of the most disruptive positions, *a* and *d*, between groups I and II, and for the fact that those positions are clustered only on one face of each interhelical interface (Fig. 7 *C*). We are, at present, unable to answer these questions.

If the SIM-1 model is correct, then there should be a structural explanation why mutations of residues from group I (positions *a* and *d*) have a greater disruptive effect on the pentamerization of helices than residues from group II. The analysis of both models reveals that each of the

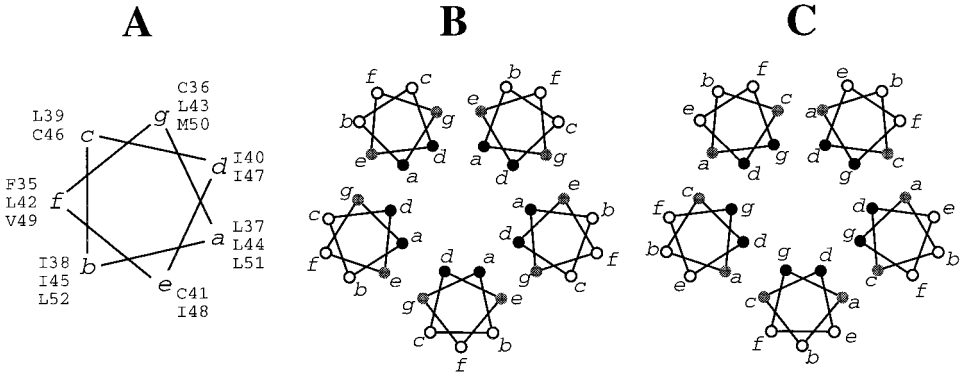

FIGURE 7 Schematic representation of the heptad repeat in PLN monomer and pentamer. (*A*) Assignment of residues 35–52 of monomeric PLN to the heptadic positions *a-g*. (*B* and *C*) Two-dimensional representation of pentameric arrangement in the SIM-1 (*B*) and ARK-1 (*C*) models. Positions classified as group I are in black, group II in grey, and groups III and IV in white (see text).

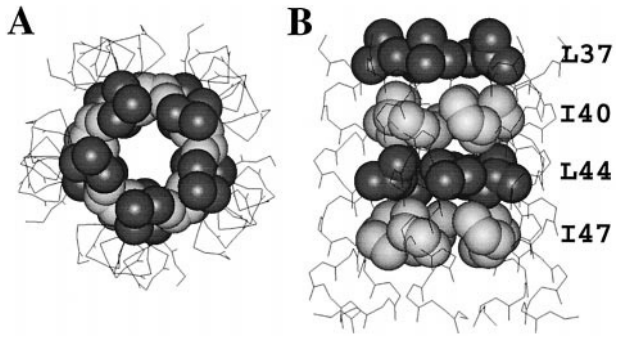

FIGURE 8 The SIM-1 model. Space-filling representation of the side chains of the residues whose mutations are classified as the most pentamer-disruptive by both mutagenesis studies (Arkin et al., 1994; Simmerman et al., 1996). (*A*) View from the cytosolic side, which shows that these residues exclusively make up the surface of the pore. (*B*) Horizontal view (cytosolic side at the *top*) showing four rings of interactions, where each of the highlighted residues interacts with its two counterparts from two neighboring helices.

group I residues interacts with two of its counterparts from two neighboring helices. In fact, these interactions form five rings, and each of them is made exclusively of the same five residues belonging to different helices. Consequently, the PLN pore is made of the stack of those rings (Fig. 8). Furthermore, no other residue in the whole TM domain interacts with its counterparts from a different helix. Thus, although the contributions to helix-helix packing from group I and group II residues are the same (Fig. 6), the effects of mutations could be different. The change in free energy upon mutation of a group I residue seems to be larger than for any other mutation, because such a mutation would affect five interactions between pairs of substituted residues. It is for that "double mutation" effect, which involves exclusively residues from group I, that one would expect the mutations of residues from group I to have the most profound effect on the oligomerization of helices. In this respect, both Arkin and Simmerman data support the hypothesis that the SIM-1 model is likely to be the correct model of the TM domain of phospholamban.

In conclusion, there is still debate on the role of phospholamban as an ion channel. However, there is considerable experimental information suggesting that the TM domain is a pentameric helix bundle, which is the central assumption made in our calculations. We have constructed two structural models for the PLN system on the basis of two distinct sets of mutagenesis data. Although one of the models provides a more rational explanation for the effect of particular mutations, the question of which of the two models is correct will be difficult to resolve until there is direct structural evidence from, for example, solid-state NMR. The calculations presented here demonstrate that comprehensive mutagenesis data combined with simple assumptions about the topology of a protein can produce structural models of high accuracy. These methods may provide alternative routes toward the elucidation of structure-function relationships for proteins, such as ion channels, for which direct structural determination is not possible.

We thank Mike J. Hartshorn for access to the Molviewer program and Leo S. D. Caves for critical reading of the manuscript.

This work was funded by the Protein Engineering LINK programme of the BBSRC, in collaboration with Glaxo-Wellcome and Division Ltd.

REFERENCES

Adams, P. D., I. T. Arkin, D. M. Engelman, and A. T. Brünger. 1995. Computational searching and mutagenesis suggest a structure for the pentameric transmembrane domain of phospholamban. *Nature Struct. Biol.* 2:154–162.

Adams, P. D., D. M. Engelman, and A. T. Brünger. 1996. Improved prediction for the structure of the dimeric transmembrane domain of glycophorin A obtained through global searching. *Proteins Struct. Funct. Genet.* 26:257–261.

Arkin, I. T., P. D. Adams, K. R. MacKenzie, M. A. Lemmon, A. T. Brünger, and D. M. Engelman. 1994. Structural organization of the pentameric transmembrane α-helices of phospholamban, a cardiac ion channel. *EMBO J.* 13:4757–4764.

Arkin, I. T., M. Rothman, C. F. C. Ludlam, S. Aimoto, D. M. Engelman, K. J. Rothschild, and S. O. Smith. 1995. Structural model of the phospholamban ion channel complex in phospholipid membranes. *J. Mol. Biol.* 248:824–834.

Bernstein, F. C., T. F. Koetzle, G. J. B. Williams, E. F. Jr. Meyer, M. D. Brice, J. R. Rodgers, O. Kennard, T. Shimanouchi, and M. Tasumi. 1977. The Protein Data Bank: a computer-based archival file for macromolecular structures. *J. Mol. Biol.* 112:535–542.

Bormann, B. J., W. J. Knowles, and V. T. Marchesi. 1989. Synthetic peptides mimic the assembly of transmembrane glycoproteins. *J. Biol. Chem.* 264:4033–4037.

Brooks, B. R., R. E. Bruccoleri, B. D. Olafson, D. J. States, S. Swaminathan, and M. Karplus. 1983. CHARMM: a program for macromolecular energy, minimization, and dynamics calculations. *J. Comp. Chem.* 4:187–217.

Brünger, A. T. 1992. X-PLOR: A System for X-ray Crystallography and NMR, version 3.1. Yale University Press, New Haven, CT.

Chothia, C., M. Levitt, and D. Richardson. 1981. Helix to helix packing in proteins. *J. Mol. Biol.* 145:215–250.

Herzyk, P., and R. E. Hubbard. 1993. A reduced representation of proteins for use in restraint satisfaction calculations. *Proteins Struct. Funct. Genet.* 17:310–324.

Herzyk, P., and R. E. Hubbard. 1995. An automated method for modelling seven-helix transmembrane receptors from experimental data. *Biophys. J.* 69:2419–2442.

Kerr, I. D., R. Sankararamakrishnan, O. S. Smart, and M. S. P. Sansom. 1994. Parallel helix bundles and ion channels: molecular modelling via simulated annealing and restrained molecular dynamics. *Biophys. J.* 67:1501–1515.

Kirchberger, M. A., M. Tada, and A. M. Katz. 1975. Phospholamban: a regulatory protein of the cardiac sarcoplasmic reticulum. *Recent Adv. Stud. Cardiac Struct. Metab.* 5:103–115.

Kirkpatrick, S., C. D. Gellat, Jr., and M. P. Vecchi. 1983. Optimization by simulated annealing. *Science.* 220:671–680.

Kovacs, R. J., M. T. Nelson, H. K. B. Simmerman, and L. R. Jones. 1988. Phospholamban forms Ca^{2+}-selective channels in lipid bilayers. *J. Biol. Chem.* 263:18364–18368.

Lemmon, M. A., J. M. Flanagan, H. R. Treutlein, J. Zhang, and D. M. Engelman. 1992. Sequence specificity in the dimerization of transmembrane α-helices. *Biochemistry.* 31:12719–12725.

Ludlam, C. F. C., I. T. Arkin, X.-M. Liu, M. S. Rothman, P. Rath, S. Aimoto, S. O. Smith, D. M. Engelman, and K. J. Rothschild. 1996. Fourier transform infrared spectroscopy and site-directed isotope labelling as a probe of local secondary structure in the transmembrane domain of phospholamban. *Biophys. J.* 70:1728–1736.

MacKenzie, K. R., J. H. Prestegard, and D. M. Engelman. 1997. A transmembrane helix dimer: structure and implications. *Science.* 276: 131–133.

Malashkevich, V. N., R. A. Kammerer, V. P. Efimov, T. Schulthess, and J. Engel. 1996. The crystal structure of a five-stranded coiled coil in COMP: a prototype ion channel? *Science.* 274:761–765.

Metropolis, N., A. W. Rosenbluth, M. N. Rosenbluth, A. H. Teller, and E. Teller. 1953. Equation of state calculation by fast computing machines. *J. Chem. Phys.* 21:1087–1092.

Neria, E., S. Fisher, and M. Karplus. 1996. Simulation of activation free-energies in molecular systems. *J. Chem. Phys.* 105:1902–1921.

Nilges, M., and A. T. Brünger. 1991. Automated modeling of coiled coils: application to the GCN4 dimerization region. *Protein Eng.* 4:649–659.

Oldfield, T. J. 1992. SQUID: a program for the analysis and display of data from crystallography and molecular dynamics. *J. Mol. Graph.* 10: 247–252.

O'Shea, E. K., J. D. Klemm, P. S. Kim, and T. Alber. 1991. X-ray structure of the GCN4 leucine zipper, a two-stranded, parallel coiled coil. *Science.* 245:539–544.

Reddy, L. G., L. R. Jones, S. E. Cala, J. J. O'Brian, S. A. Tutalian, and D. L. Stokes. 1995. Functional reconstitution of recombinant phospholamban with rabbit skeletal Ca^{2+}-ATPase. *J. Biol. Chem.* 270: 9390–9397.

Simmerman, H. K. B., Y. M. Kobayashi, J. M. Autry, and L. R. Jones. 1996. A leucine zipper stabilizes the pentamer membrane domain of phospholamban and forms a coiled-coil pore structure. *J. Biol. Chem.* 271:5941–5946.

Simmerman, H. K. B., D. E. Lovelace, and L. R. Jones. 1989. Secondary structure of detergent-solubilized phospholamban, a phosphorylatable, oligomeric protein of cardiac sarcoplasmic reticulum. *Biochim. Biophys. Acta.* 997:322–329.

Smith, S. O., and B. J. Bormann. 1995. Determination of helix-helix interactions in membranes by rational resonance NMR. *Proc. Natl. Acad. Sci. USA.* 92:488–491.

Tada, M., and M. Kadoma. 1989. Regulation of the Ca^{2+}-pump ATPase by cAMP-dependent phosphorylation of phospholamban. *BioEssays.* 10: 157–163.

Treutlein, H. R., M. A. Lemmon, D. M. Engelman, and A. T. Brünger. 1992. The glycophorin A transmembrane domain dimer: sequence-specific propensity for a right-handed supercoil of helices. *Biochemistry.* 31:12726–12733.